Journal of Applied Sciences

ISSN 1812-5654

science alert

ANSInet
an open access publisher
http://ansinet.com

Journal of Applied Sciences 9 (15): 2671-2687, 2009
ISSN 1812-5654

Geochemistry and Petrogenesis of Mantle Peridotites from the Nehbandan Ophiolitic Complex, Eastern Iran

[1]M. Delavari, [1]S. Amini, [2]E. Saccani and [2]L. Beccaluva
[1]Department of Geology, Faculty of Science, Tarbiat Moallem University, Tehran, Iran
[2]Dipartimento di Scienze Della Terra, Università di Ferrara, Via Saragat 1, 44100 Ferrara, Italy

Abstract: Ophiolitic exposures from the East and Northeast of Nehbandan, Eastern Iran, are remnants of a Cretaceous oceanic basin between Lut and Afghan continental blocks. Based on petrographic studies, they contain harzburgite, clinopyroxene-harzburgite and lherzolite equilibrated in spinel peridotite facies. Chemistry of clinopyroxene in lherzolite is characterized by low Na_2O and TiO_2 contents suggesting sub-oceanic origin. Spinel is a ubiquities accessory phase yielding chromium number [Cr# = 100*Cr/(Cr+Al)] in the range of 31-37 and 15-21 for harzburgite and lherzolite, respectively. Melting degrees on the basis of spinel chemistry is 5 to 8% for lherzolite and 12.5 to 14.2% for harzburgite. Cr# of magmatic spinel is 50-51 which correlate with Al-rich type of podiform chromitites. Whole-rock chemistry shows that most of the peridotitic samples exhibit evident U-shaped primitive mantle-normalized rare earth element patterns. In addition, in multi-element diagrams, relative to neighboring rare earth elements, Nb and Ta are highly enriched accompanied by to a lesser extent Th and U enrichments. The geochemical features represent mantle-melt interactions and contamination with continental sources. Geodynamically, the mantle tectonites record both mid-ocean ridge and supra-subduction zone signatures.

Key words: Spinel, melting, HFSE enrichment, harzburgite, lherzolite

INTRODUCTION

Mantle peridotites generally occur on Earth surface as orogenic peridotites involved in mountain belts, xenoliths entrained in mafic alkaline magmas, abyssal peridotites dredged or drilled from the modern oceanic floors and mantle section of ophiolites. In this perspective, as ophiolites represent preserved parts of tectonically emplaced oceanic lithosphere, widely exposed parts of oceanic upper mantle are accessible in ophiolitic associations worldwide and many investigations have been focused on the mantle section of ophiolitic complexes (Godard *et al*., 2000; Tamura and Arai, 2006; Pagé *et al*., 2007).

Using both whole-rock and mineral compositions of mantle peridotites help us to discuss about the relevant petrogenetic processes and make some assumptions on their tectonomagmatic environment as mantle section of ophiolites may represent oceanic lithosphere formed in Mid-Ocean Ridge (MOR) or Supra-Subduction Zone (SSZ) settings. Specially, the chemical composition of chrome spinel is a useful indicator which afford discussing about geodynamic setting or evaluating refractoriness degree of mantle peridotites (Dick and Bullen, 1984; Arai, 1994; Zhou *et al*., 1996, 1998; Kamenetsky *et al*., 2001; Büchl *et al*., 2004; Arif and Qasim Jan, 2006; Karipi *et al*., 2007). In this study, new geochemical data from the mantle section of the Nehbandan ophiolite, Eastern Iran, are given. In Eastern Iran, ophiolitic remnants are highly exposed but have received little attention and remained largely unknown. Detailed investigations have not yet been carried out to shed light on the issues regarding the geochemical-petrological characterization of the crust and mantle suites and the geodynamic setting of ophiolite formation. Present data set includes major and trace elements of whole-rock samples and microprobe data of mineral phases. The objective of the study is to concentrate on mantle peridotites for the sake of elucidating their petrological characteristics.

MATERIALS AND METHODS

The chemical analysis are conducted in September to December 2007. Major element compositions of minerals were determined by electron microprobe analysis (EMPA), using a Cameca CAMEBAX instrument, at the Istituto di Geoscienze e Georisorse, CNR, Padua (Italy). An acceleration voltage of 15 keV and sample currents of 20 μA with 100 sec counting time was used. Oxides, as

Corresponding Author: M. Delavari, Department of Geology, Faculty of Science, Tarbiat Moallem University, Tehran, Iran

well as natural and synthetic minerals were used as standards. Matrix corrections were performed using the PAP program supplied by Cameca. Analytical precision (2σ) is better than ±2% for elements in the range 10-20 wt.% oxide, better than 5% for elements in the range 2-10 wt.% oxide and better than 10% for elements in the range 0.5-2 wt.% oxide.

Whole-rock major and some trace elements (Sc, Ga, Ni, Co, Cr, V, Ba, Th, Nb, Zr, Y) were obtained by X-Ray Fluorescence (XRF) on pressed-powder pellets, using an ARL Advant-XP automated X-ray spectrometer, at the Dipartimento di Scienze della Terra, Università di Ferrara (Italy). Calibration was done using international reference samples (some of which were also run as unknowns for the determination of accuracy and detection limits) and the matrix correction method proposed by Lachance and Trail (1966) was applied. Mean accuracies are generally less than 2% for major oxides and 5% for trace element determinations, while the detection limits for trace elements are: Ba = 5 ppm; Ni, Co, Cr, V = 1 ppm; Zr, Y = 2 ppm. Volatile contents were determined as loss on ignition at 1000°C.

In addition, Y, Zr, Nb, Hf, Ta, Th and U and the Rare Earth Elements (REE) were determined by Inductively Coupled Plasma-Mass Spectrometry (ICP-MS) using a VG Elemental Plasma Quad PQ2 Plus spectrometer, at the Dipartimento di Scienze della Terra, Università di Ferrara (Italy). The accuracy of the data and detection limits were evaluated using results for international standard rocks and the blind standards included in the sample set. Accuracy ranges from 2 to 7 relative percent, with the exception of Nb and Ta (12%) and U (9%). Detection limits (in ppm) are: Sc = 0.29; Nb, Hf, Ta = 0.02; Th, U = 0.01; La, Lu, Tm = 0.10; Ce, Ho = 0.20; Pr, Sm, Gd, Dy, Er, Yb = 0.02; Nd = 0.07; Eu, Tb = 0.01. All whole-rock analyses were performed at the Department of Earth Science of the University of Ferrara.

RESULTS

Regional geology and field evidences: In Iran, ophiolitic exposures are nearly widespread which have been formed in several sutured zones witnessing the vestiges of ancient Tethyan Ocean in central part of Alpine-Himalayan belt (Fig. 1a). The East Iranian Ranges called by Tirrul *et al.* (1983) as Sistan suture zone is an orogenic belt delimited by two continental blocks; Lut block to the west and Afghan block to the east (Fig. 1a). This zone which encompasses some mafic-ultramafic associations was considered as a branch of Neo-Tethys extending from central Makran Ranges northward to Birjand area which opened and closed in the time interval of upper Cretaceous (Tirrul *et al.*, 1983). Ophiolitic remnants preserving both mantle and crustal lithologies occur as discrete massifs along the Sistan suture zone. The study area is located to the North of the Tchehel Kureh ophiolite and to the East and Northeast of Nehbandan town herein referred to as Nehbandan Ophiolite Complex (NOC) (Fig. 1b). In NOC, exposures of mantle rocks are more abundant. The smooth to rugged topographic highs are commonly made by mantle rock occurrences. During later tectonic accretions, in some places the mantle exposures were thrusted onto younger clastics of Tertiary. The mantle tectonites have been locally cut by numerous patches and dykes (Fig. 2a-f) of gabbro-dolerite, gabbronorite, basalt and also rare troctolitic dykes. The contact between magmatic bodies and host peridotite is always sharp implying in the course of late magmatic intrusion the host mantle was in cold lithospheric condition. The mafic patches are variable in size and reach up to 50 m in diameter. Petrographically, the gabbroic and gabbronoritic patches are medium to coarse-grained and sometimes show deformation attributes manifested by distorted mineral phases. The gabbros are characterized by crystallization of plagioclase prior to clinopyroxene and in gabbronorites plagioclase appear later than pyroxene (ortho- and clinopyroxene) in crystallization sequence. The products of hydrothermal alteration are easily visible as dyke-like masses of light-colored carbonatized-silicified serpentine (listwaenite) which sporadically crosscut the mantle peridotites and made it possible many exploitable magnesite mines to be formed. Passing through mantle to crustal rocks are nowhere intrusive or gradational. The observed ultramafic cumulates including pyroxenite and dunite lie with faulted contact near mantle rocks. In outcrop area, they are confined to thin less than 300 m thick units. Mafic crustal cumulates comprising gabbro and gabbronorite have wider exposures compared to other crustal units but they don't show typical layered structures. High level gabbro and dolerite are less abundant. In some parts high-level gabbros have been cut by irregular network of plagiogranitic apophyses, dykes and veins.

Sheeted dykes are difficult to be observed may be their original extent has been much reduced by erosion. Mafic volcanic complex in NOC contains both massive and pillowed basalts. In pillowed basalt, the pillows are diverse in size and reach up to 2 m in diameter. Passing upward no sedimentary cover rest on pillowed flows and massive basalts but several solitary blocks of pelagic limestone can be found. The microfauna of these limestones have yielded late Turonian age. Lithological relationships show that ophiolite emplacement occurred in late Cretaceous but deep-water sedimentation continued to early Eocene after that collision between Lut

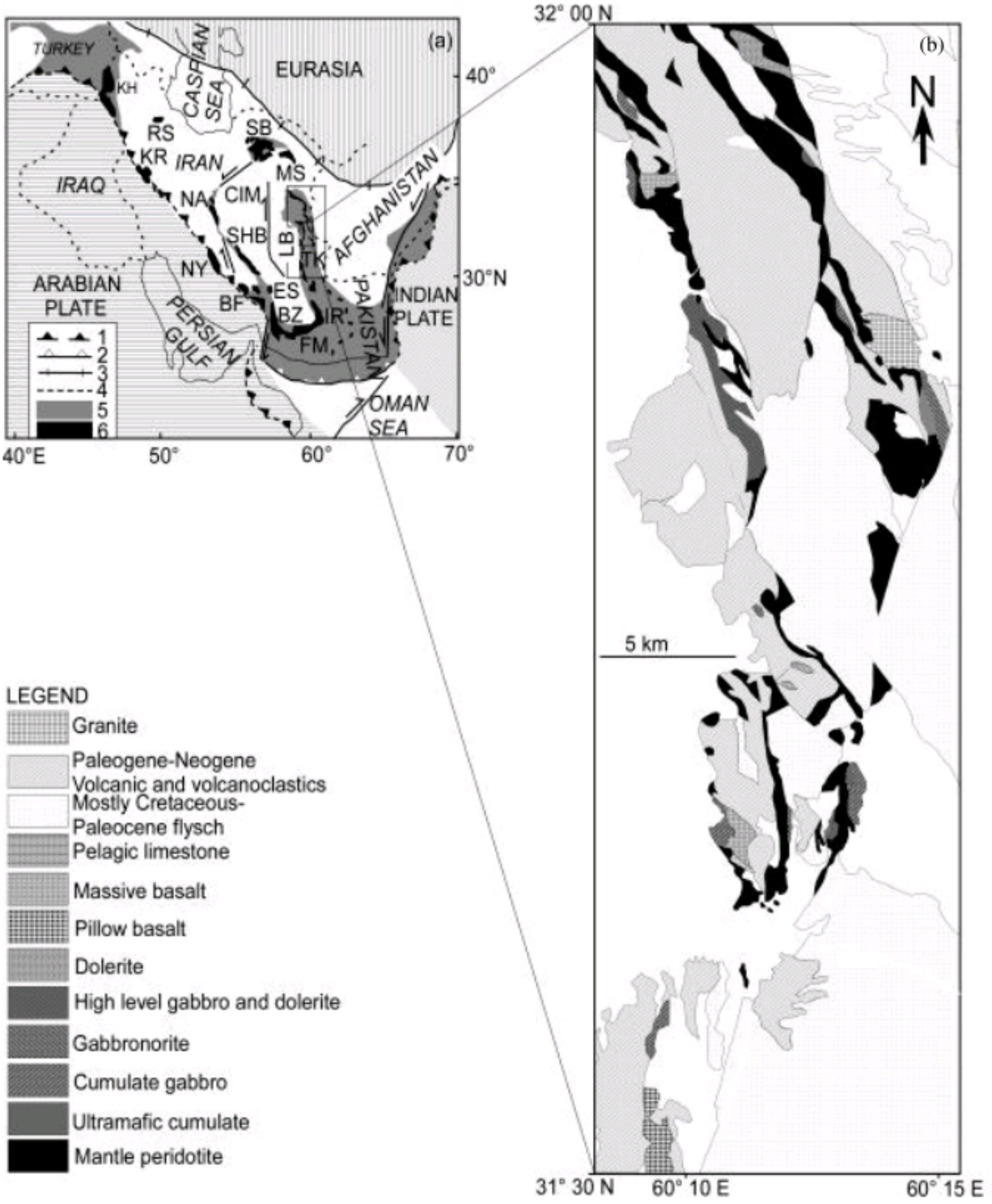

Fig. 1: (a) Generalised tectonic map of the Middle East showing location of the Sistan suture zone (the box between the Lut Block (LB) and Afghan block). 1 : Neo-Tethyen suture, 2: Active trench, 3: Paleo-Tethyan suture, 4: Borders, 5: Neo-Tethyan accretionary complex, 6: Ophiolitic remnants, CIM: Central Iran microcontinent which includes Lut block as its Eastern part. Also, locations of major Iranian ophiolites are given: BF: Baft; BZ: Band-e-Zeyarat; ES: Esphandagheh; FM: Fanuj-Maskutan; IR: Iranshahr; KH: Khoy; KR: Kermanshah; MS: Mashad; NA: Nain; NY: Neyriz; RS: Rasht; SB: Sabzevar; SHB: Shahr-Babak; TK: Tchehel Kureh. Study area (small box) expanded in Fig. 1b. (b) simplified geological map of the study area (modified after Tirrul *et al*., 1989).

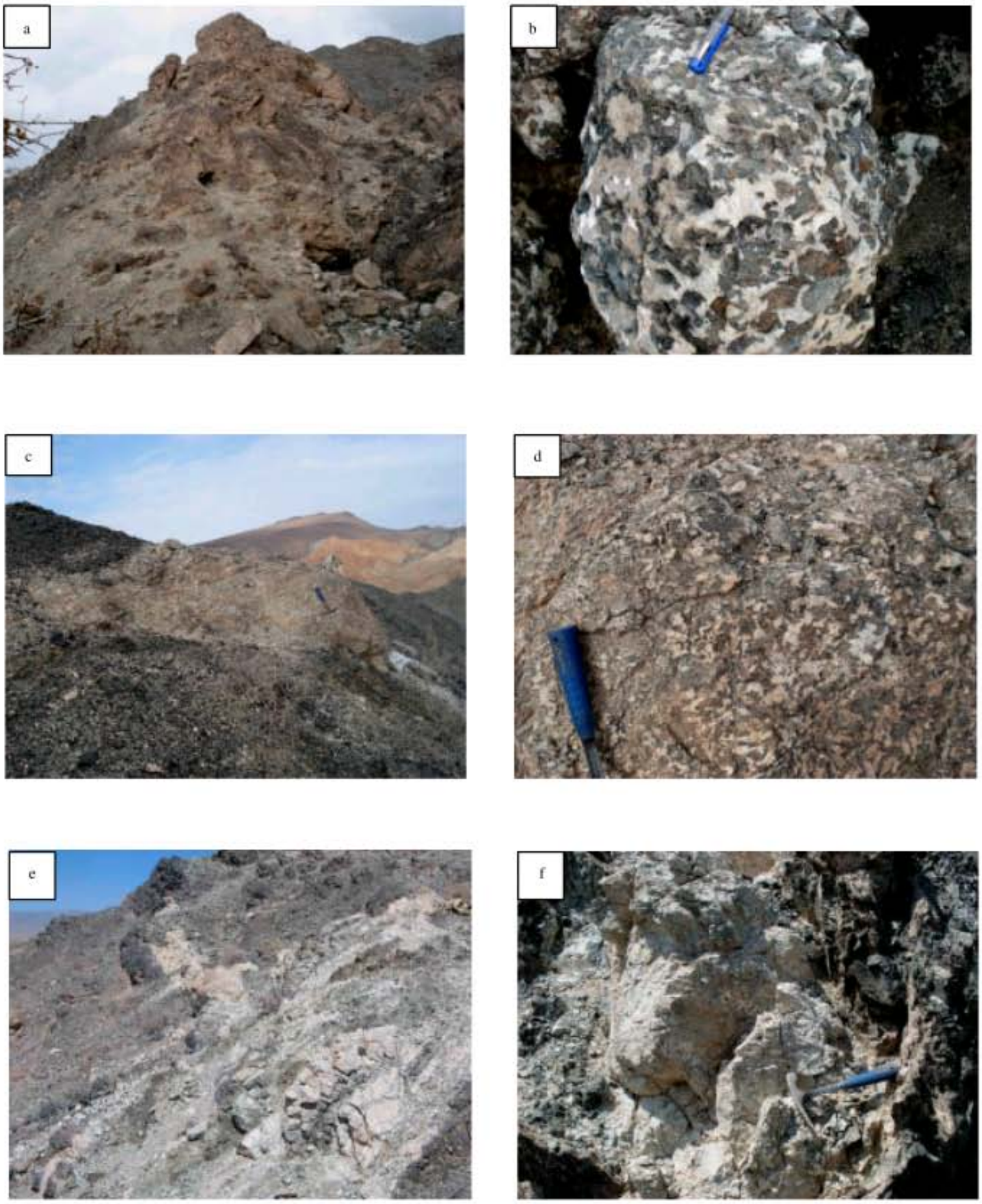

Fig. 2: Field photographs substantiating solidified mafic magmas inside host peridotites. (a) and (c) gabbronorite patches intruded into mantle peridotites. The maximum width of the patch in (a) is around 10 m. (b) and (d) are close views of (a) and (c), respectively. In (b) and (d) earlier crystallization of pyroxene relative to plagioclase is apparent as plagioclase fills the interstices of pyroxenes. (e) Mantle peridotite crosscut by troctolite dyke. The thickness of dyke in the part pointed out by arrow is 0.5 m. (f) Gabbro inside mantle tectonites. They range in size from thin dykes up to some tens of meters-wide lenses mainly with sharp contacts

Table 1: Representative analyses of olivine, orthopyroxene, clinopyroxene and spinel

Rock type	Harzburgite		Lherzolite		Rock type	Lherzolite			Harzburgite			Rock type	Harzburgite		Lherzolite		Chromitite	
Sample	4-44		6-38		Sample	6-38			4-44			Sample	4-44		6-38		4-40	
Site-mineral	4-ol2	7-ol3	1-ol10	6-ol1	Site-mineral	1-cpx3	7-cpx1	3-cpx1	3-opx3	3-opx1	7-opx2	Site-mineral	2-sp5	4-sp2	1-sp4	2-sp2	1-sp2	2-sp10
SiO_2	41.32	41.45	41.73	41.67	SiO_2	52.25	52.50	54.27	55.46	56.58	56.27	SiO_2	0.03	0.03	2.97	0.10	0.04	0.09
TiO_2	0.02	0.00	0.00	0.00	TiO_2	0.23	0.19	0.03	0.08	0.05	0.04	TiO_2	0.05	0.01	0.05	0.03	0.06	0.13
Al_2O_3	0.03	0.01	0.03	0.03	Al_2O_3	4.10	5.00	5.16	4.32	3.05	2.89	Al_2O_3	40.23	36.94	50.47	48.85	27.47	26.82
Cr_2O_3	0.08	0.00	0.02	0.01	Cr_2O_3	0.86	1.09	0.79	0.63	0.76	0.61	Cr_2O_3	28.21	31.27	13.56	18.90	41.30	41.97
FeO	8.81	9.46	9.93	10.40	FeO	2.06	3.08	6.65	6.78	5.82	5.84	Fe_2O_3	1.33	1.66	0.00	1.07	2.14	2.34
Mno	0.07	0.18	0.16	0.16	MnO	0.01	0.11	0.06	0.10	0.15	0.19	FeO	14.83	15.72	15.25	13.87	13.98	13.59
MgO	49.44	48.94	48.41	48.92	MgO	15.82	18.68	31.89	32.12	32.06	33.55	MnO	0.13	0.19	0.21	0.02	0.26	0.21
CaO	0.02	0.01	0.02	0.00	CaO	24.50	19.75	1.09	1.42	2.28	0.90	MgO	15.31	14.33	15.64	16.87	14.40	14.75
Na_2O	0.00	0.00	0.02	0.03	Na_2O	0.24	0.20	0.02	0.00	0.00	0.03	CaO	0.00	0.00	0.03	0.01	0.00	0.00
NiO	0.35	0.35	0.47	0.37	K_2O	0.04	0.02	0.00	0.00	0.00	0.00	NiO	0.19	0.20	0.26	0.17	0.12	0.16
Total	100.14	100.40	100.80	101.59	Total	100.12	100.62	99.95	100.90	100.74	100.33	Total	100.29	100.35	98.45	99.91	99.76	100.05
Si	1.006	1.010	1.014	1.007	Si	1.900	1.883	1.882	1.906	1.943	1.935	Si	0.001	0.001	0.080	0.003	0.001	0.003
Ti	0.000	0.000	0.000	0.000	Ti	0.006	0.005	0.001	0.002	0.001	0.001	Ti	0.001	0.000	0.001	0.001	0.001	0.003
Al	0.001	0.000	0.001	0.001	Al	0.176	0.211	0.211	0.175	0.123	0.117	Al	1.343	1.257	1.610	1.569	0.975	0.951
Cr	0.002	0.000	0.000	0.000	Cr	0.025	0.031	0.022	0.017	0.021	0.017	Cr	0.632	0.714	0.290	0.407	0.984	0.998
Fe^{2+}	0.179	0.193	0.202	0.210	Fe^{3+}	0.003	0.000	0.003	0.000	0.000	0.000	Fe^{3+}	0.028	0.036	0.000	0.022	0.048	0.053
Mn	0.002	0.004	0.003	0.003	Fe^{2+}	0.060	0.093	0.189	0.195	0.167	0.168	Fe^{2+}	0.350	0.378	0.345	0.315	0.350	0.340
Mg	1.795	1.777	1.754	1.763	Mn	0.000	0.003	0.002	0.003	0.004	0.006	Mn	0.003	0.005	0.005	0.000	0.007	0.005
Ca	0.001	0.000	0.000	0.000	Mg	0.857	0.999	1.648	1.646	1.641	1.720	Mg	0.646	0.617	0.631	0.686	0.647	0.661
Na	0.000	0.000	0.001	0.002	Ca	0.955	0.759	0.040	0.052	0.084	0.033	Ca	0.000	0.000	0.001	0.000	0.000	0.000
Ni	0.007	0.007	0.009	0.007	Na	0.017	0.014	0.002	0.000	0.000	0.002	Ni	0.004	0.005	0.006	0.004	0.003	0.004
Total	2.992	2.990	2.986	2.993	K	0.002	0.001	0.000	0.000	0.000	0.000	Total	3.009	3.012	2.969	3.007	3.016	3.017
Fo	90.840	90.050	89.530	89.200	Total	4.001	3.999	4.000	3.996	3.984	3.998	Cr#	31.990	36.220	15.280	20.610	50.210	51.210
Fa	9.080	9.770	10.300	10.630								Mg#	62.990	59.740	64.640	66.970	61.730	62.620

ol: Olivine, cpx: Clinopyroxene, opx: Orthopyroxene, sp: Spinel

block and trench completely closed the basin and resulted in structural thickening and regional uplifts. Despite many typical Tethyan ophiolites which have been emplaced as intact nappes onto adjacent continental margin (Oman ophiolite), the mode of ophiolite emplacement in Sistan suture zone is as dismembered ophiolitic blocks and offscraped slices incorporated into diverse younger lithologies.

Petrography and mineral chemistry: The mantle sequence of NOC is dominated by harzburgite and lherzolite which based on clinopyroxene frequency they can be classified as harzburgite, cpx-harzburgite and lherzolite/cpx-rich harzburgite. Mantle peridotites have mainly equigranular to inequigranular porphyroclastic texture. Fusion related features are characterized by amoeboid grain shapes or uneven contacts between adjoining olivine-olivine or olivine-pyroxene grains in which the grains enter as corridors into each other. High temperature ductile deformation is evident in some of the samples. The mantle peridotites underwent varying degrees of alteration mainly in the form of transformation into serpentine polymorphs and iron oxide during or after accretionary uplift. Some samples are nearly fresh reflected in their low LOI contents (less than 5%). Table 1 shows representative analysis of mineral phases.

Olivine: Olivine forms 70 to 85% of the mode and appears as up to 3 mm sized porphyroclasts to finer <1 mm grains. It occasionally exhibits deformational features such as kink band, undulatory extinction and sub-grains. Although, olivine is the least alteration resistant phase and in altered samples it was hardly replaced by serpentine, in slightly altered samples completely fresh olivine can be observed. Iron oxide is another frequent disintegration product which occurs as very fine to coarser opaque spots enclosed in serpentine. Olivine grains are usually unzoned and homogeneous. Serpentinization along grain boundaries and fractures has been led to a mesh-texture which is very common in altered mantle peridotites. In harzburgite, olivine doesn't show wide compositional variations and ranges from Fo_{90} to Fo_{91}. NiO is relatively high (0.25-0.56 wt.%) and CaO is close to the detection limit (<0.05 wt.%). In lherzolite, olivine has narrow and lower Fo ranges (Fo_{89} to $Fo_{89.5}$). NiO and CaO contents are from 0.32 to 0.61 wt.% and <0.03 wt.%, respectively.

Orthopyroxene: In NOC mantle peridotites, orthopyroxene forms 10 to 25% of the rock volume. Orthopyroxene porphyroclasts have generally irregular outlines sometimes with sub-spherical shape. They are mainly less than 2 mm but infrequently attain up to 6 mm in diameter which appear as the largest grains among the constituent phases and sometimes can also be recognized in hand specimens. Kink-band, curved cleavage and undulatory extinction are reminiscent of strain-related features (Fig. 3b-d). Clinopyroxene in the form of blebs and exsolution lamellae parallel to (100) and inclusions of olivine and Cr-spinel can be seen in orthopyroxene.

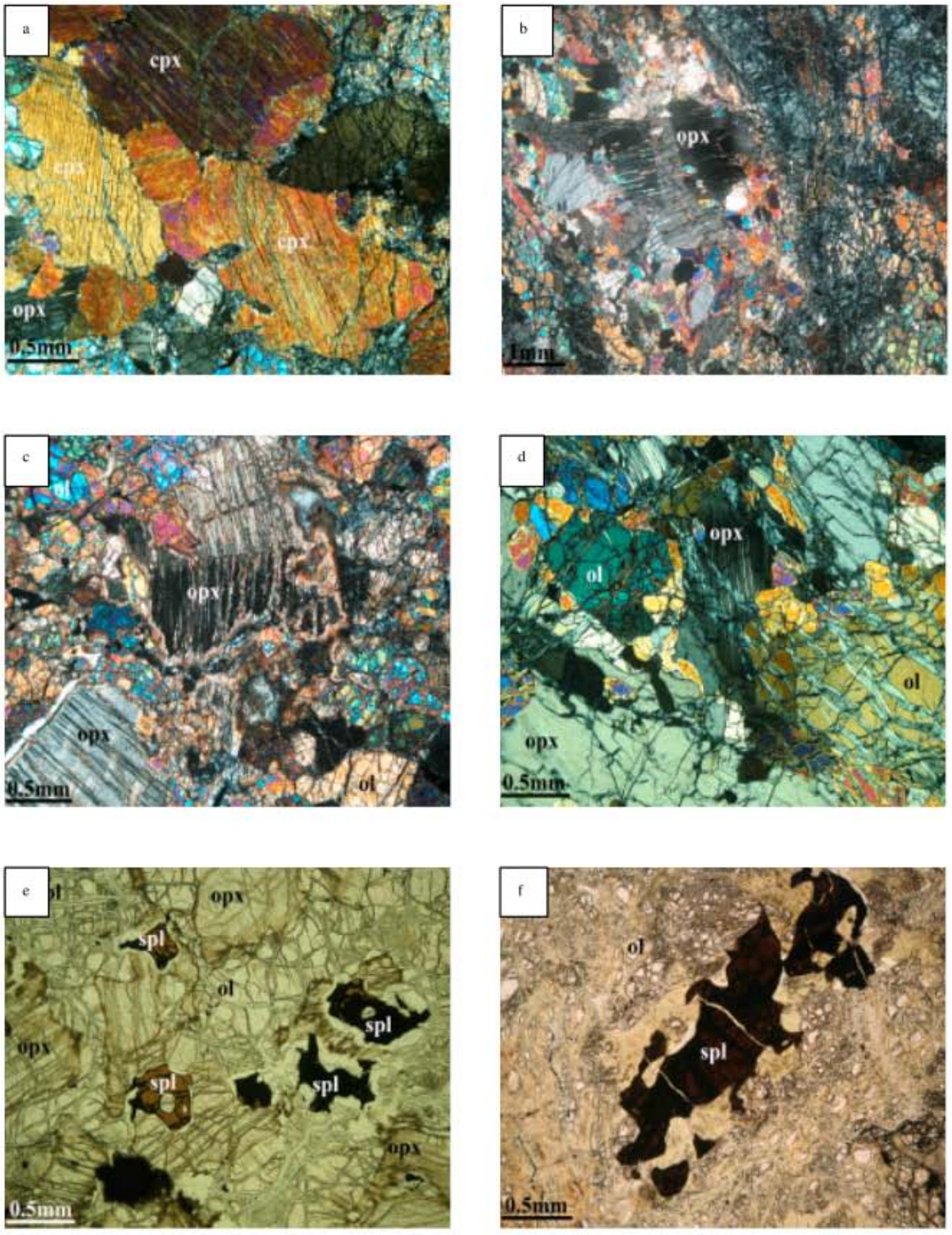

Fig. 3: Photomicrographs of NOC mantle peridotites. (a) Clinopyroxene porphyroclasts in lherzolite with thin orthopyroxene exsolution lamellae, (b) and (c) kink band texture in orthopyroxene and sub-grains of olivine showing high-temperature deformation in mantle peridotites, (d) Approximately fresh harzburgite with curved orthopyroxene suggesting ductile deformation, (e) and (f) fresh to altered anhedral Cr-spinel grains with lobate boundaries. The fresh ones are brown to reddish-brown and altered ones are completely dark in color. (a) to (d) in crossed-polarized light, (e) and (f) in plane-polarized light

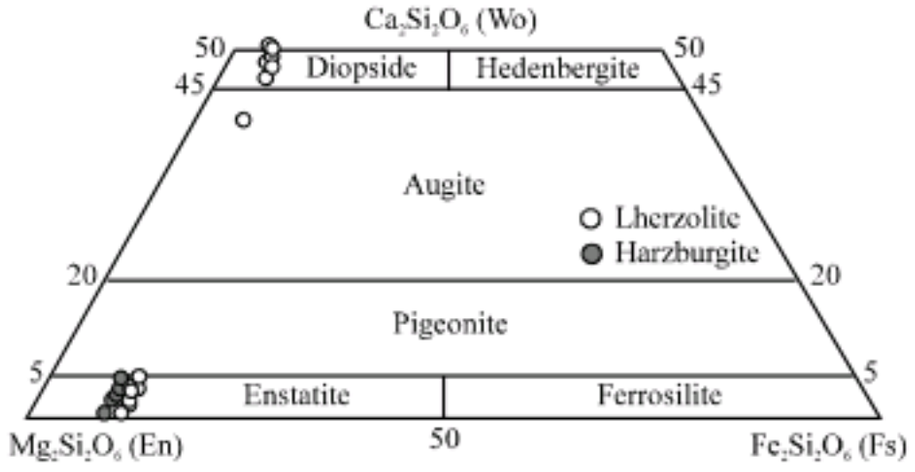

Fig. 4: Pyroxene ternary diagram (Morimoto, 1989) showing clinopyroxene and orthopyroxene composition of the mantle peridotites

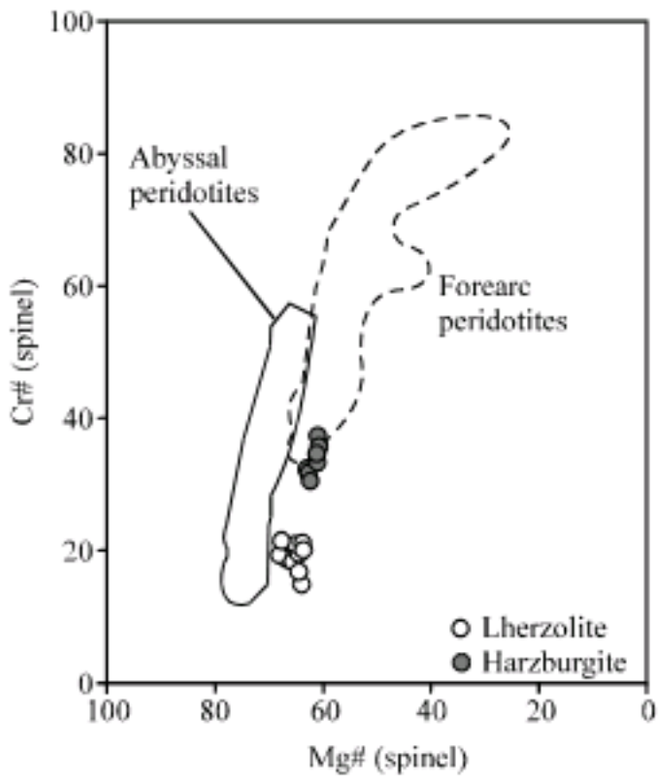

Fig. 5: Cr# vs. Mg# for Cr-spinels. Field of abyssal peridotite after Dick and Bullen (1984) and Niu and Hékinian (1997) and that of forearc peridotite after Ishii *et al*. (1992) and Parkinson and Pearce (1998)

In altered samples, orthopyroxene is usually replaced by bastite. The orthopyroxene is compositionally Mg-rich enstatite with Mg-numbers of 90.5-92.6 and 89.1-90.3 in harzburgite and lherzolite, respectively. The composition of orthopyroxene can be seen in Fig. 4 which is in the ranges of $En_{88.5–90.2}$ $Fs_{9–9.7}$ $Wo_{1–2}$ and $En_{84.5–88.5}$ $Fs_{9.5–10.5}$ $Wo_{1–5}$ in harzburgite and lherzolite, respectively. Additionally, harzburgitic orthopyroxene has lower Al_2O_3 (2.77-3.26 wt.%) and TiO_2(<0.01-0.08) contents relative to lherzolitic orthopyroxene with Al_2O_3 and TiO_2 contents in the range of 4.32-5.22 wt.% and 0.03-0.12 wt.%, respectively.

Clinopyroxene: Clinopyroxene ranges modally from less than 1% to more than 5%. Clinopyroxene appears as isolated grain or aggregate and is variable in size ranging from less than 1 mm to up to 3 mm in diameter (Fig. 3a). It almost shows exsolution lamellae of orthopyroxene and normally has corroded boundaries. The clinopyroxene in lherzolite has high Al_2O_3 contents with limited variation (~4.2-4.9 wt.%). Mg# shows substantial variation and is 92.0 to 98.6. In pyroxene ternary diagram (Fig. 4) the clinopyroxenes plot in diopside field with a composition of $En_{45–49}$ $Fs_{3.2–4.6}$ $Wo_{46.5–51}$. Moreover, they have low Na_2O (0.16-0.31 wt.%) and TiO_2 (0.19-0.35 wt.%) contents which is similar to clinopyroxenes of abyssal peridotites (Johnson *et al*., 1990) reinforcing their sub-oceanic provenance.

Cr-spinel: Cr-spinel inside harzburgite and lherzolite is modally less than 1% and appears as a ubiquitous accessory phase. It usually occurs as small (<1 mm) grain but occasionally is larger (up to 2 mm). The spinel always shows lobate boundaries implying residual origin (Fig. 3e, f) leaving after partial melting of the mantle peridotites. When occurring as inclusion inside orthopyroxene, it may have subhedral to euhedral shape. Cr-spinel is sometimes altered to Fe-rich spinel along margins and fractures and occasionally is completely altered. Fresh Cr-spinel is typically reddish-brown in color and ranges to dark when it is altered to ferritchromite (Fig. 3e). In harzburgite, the Cr-spinel is characterized by Mg# ($100\times Mg/(Mg+Fe_2^+)$) and Cr# ($100\times Cr/(Cr+Al)$) of 59.7 to 64 and 31.6 to 37.5, respectively. Lherzolitic Cr-spinel has higher Mg# (63.4-68.2) and lower Cr# (15.3-21). Additionally, TiO_2 content of harzburgitic Cr-spinel is 0.01 to 0.06 wt.% which is lower compared to lherzolitic Cr-spinel having TiO_2 content ranging from 0.03-0.1 wt.%. As it is clear Mg# in spinel from less depleted peridotites (lherzolite) is higher than that of more depleted peridotites (harzburgite) a feature that is common in Cr-spinels inside peridotites (Fig. 4).

Among the phases constitute mantle peridotites; spinel is relatively more resistant to alteration. Cr# of spinel specially seems to remain constant during subsolidus stages (Arai, 1994). Therefore, chemical composition of spinel can be used as the basis for many discriminate diagrams appropriate for the study of geotectonic setting of host mantle peridotites. Figure 5 shows the Cr# vs. Mg# diagram in which harzburgitic Cr-spinel is in compositional ranges similar to abyssal peridotites or least depleted forearc peridotites and lherzolitic Cr-spinel plots close to the fertile end of abyssal peridotites.

Additionally, the mantle exposures in Sistan suture zone host numerous chromitite ores. Here, the studied samples are taken from Bandan mine located to the southeast of study area. The chromite deposits mostly appear as fault bounded ores in mantle tectonites having

unclear relations with the host peridotite. Chromitite is texturally nodular, massive to disseminated and chromite grains are less than 2 mm to 1 cm in size. The chromites have Cr# of 50-51 which lie within the Cr# ranges of ophiolitic chromitite deposits (Zhou *et al*., 1996, 1998) and correlate with Al-rich type of podiform chromitites. Mg# and TiO_2 content are 60.5-63 and 0.07-0.17 wt.%, respectively.

Geothermometry: Using several geothermometers, we tried to obtain equilibration temperatures for coexisting mineral phases of mantle peridotites. In harzburgite, assuming a 20 Kbar pressure, the orthopyroxene geothermometer of Brey and Köhler (1990) indicate the temperatures of about 1000-1100°C. Additionally, orthopyroxene geothermometer of Witt-Eickschen and Seck (1991) yielded the temperature in the range of 1010-1030°C. Applying orthopyroxene geothermometer of Brey and Köhler (1990) the temperatures of 1200 to 1220 was obtained for lherzolite. Additionally, the orthopyroxene geothermometer of Witt-Eickschen and Seck (1991) yielded the temperatures of about 1120 to 1125°C for lherzolite. The presence of clinopyroxene in lherzolite allows us to use clinopyroxene-orthopyroxene geothermometers of Brey and Köhler (1990) and Wells (1977) which show the temperature of 1200-1250 and 1050-1150°C, respectively. Reviewing the upper-mentioned results reveals that the calculated temperatures are clearly lower than the expected equilibration temperatures of mantle peridotite mineral phases so they reflect subsolidus re-equilibration temperatures. Furthermore, in lherzolite the yielded temperatures are relatively higher than those of harzburgite. Because NOC mantle peridotites have experienced dislocations and the initial stratigraphical orders are not preserved, higher re-equilibration temperature of lherzolite may imply their deeper origin.

Geochemistry: Table 2 represents the whole rock major and trace elements of the samples. Ophiolitic mantle peridotites are commonly highly altered. LOI (Loss On Ignition) contents in NOC mantle peridotites range from 4 to 7 wt.% which are nearly high in some samples so we used recalculated anhydrous whole rock data for geochemical interpretations. Anhydrous SiO_2 content in harzburgite and lherzolite ranges from 41.75 to 43 wt.% and 42.75 to 43.15 wt.%, respectively. Al_2O_3 and CaO contents in harzburgite are in the ranges of 1.0 to 1.7 wt.% and 0.7 to 1.15 wt.%, respectively. In lherzolite, Al_2O_3 and CaO contents range from 1.8 to 2.3 wt.% and 1.63 to 2.15 wt.%, respectively. The CaO/Al_2O_3 ratio in peridotites has narrow range and changes from 0.66 to 1.06 in harzburgite and 0.76 to 1.02 in lherzolite. MgO in harzburgite is 41.1-43.35 wt.% and in lherzolite is 40-41.7 wt.%. Na_2O and TiO_2 contents are lower in harzburgite and are in the ranges of 0.01 to 0.04 wt.% and <0.01 to 0.02 wt.%, respectively. In lherzolite, Na_2O is 0.04-0.07 wt.% and TiO_2 is 0.02-0.03 wt.%. In co-variation diagram of major element oxides (Fig. 6a-e) all the data plot within the field of mantle peridotites (orogenic, abyssal and ophiolitic) (Bodinier and Godard, 2003). As can be seen, in NOC samples along with mantle peridotites, SiO_2 do not show good coherent co-variation with Al_2O_3 but MgO, CaO, TiO_2 and Na_2O show positive correlation with Al_2O_3 between a more fertile and a more refractory end-members. Major element oxide variations are clearly due to different modal compositions. As it is expected these variations can imply variable degrees of partial melting of the mantle peridotites although, small-scale modal heterogeneity, secondary alteration processes, mantle metasomatism and melt-rock interaction prior to tectonic emplacement may have important role on compositional variations of mantle peridotites (Bodinier and Godard, 2003).

In MgO/SiO_2 vs. Al_2O_3/SiO_2 diagram (Fig. 7), the data plot a little below but close and parallel to the terrestrial array suggesting melting trend of a primitive mantle composition (Jagoutz *et al*., 1979). The relatedness between plotted data and the terrestrial array coupled with major element co-variation trends reveal genetical relationship between variously depleted NOC mantle peridotites in which melting process acted as a main factor in their evolutionary trend. Although, it must be noted that the fertile nature of mantle peridotites may be related to diminished melting degrees or clinopyroxene forming refertilization process (Godard *et al*., 2000; Takazawa *et al*., 2003).

Figure 8 shows the Primitive Mantle (PM) normalized (Sun and McDonough, 1989) Rare Earth Elements (REE) and trace elements patterns of analysed samples. One of the important aspects of the patterns is the enrichment of High Field Strength Elements (HFSEs). In harzburgite, Th, U, Nb and Ta represent enrichment compared to REE and in some samples Nb and Ta are even more enriched than PM composition. In addition, Zr, Hf and Ti display marked spikes relative to neighboring REEs. Like harzburgite, lherzolitic samples demonstrate conspicuous Th, U, Nb and Ta enrichments in comparison with LREE and MREE especially regarding the sample 2-20 which shows unusual Nb and Ta enrichment. Moreover, the sample 2-20 shows noticeable Hf and Ti pikes. The U/Th ratio is always more than primitive mantle value and is ~ 1-7 × primitive mantle in harzburgite and ~ 1-5 × primitive mantle

Table 2: Major and trace element analysis of mantle peridotites

	Samples										
	4--45	2--34	3--37	4--44	4--15	2--20	2--33	4--10	6--38	5--6	4--11
	Rocks										
Elements	CPX-HZ	HZ	CPX-HZ	HZ	HZ	Lhrz	Lhrz	Lhrz	Lhrz	Lhrz	CPX-HZ
XRF analysis (wt.%)											
SiO_2	42.18	42.18	41.76	43.03	42.98	43.14	43.08	43.15	42.76	42.84	42.83
TiO_2	0.00	0.01	0.01	0.01	0.01	0.02	0.02	0.03	0.03	0.03	0.02
Al_2O_3	0.98	0.91	0.96	1.15	1.25	1.71	1.86	2.02	1.96	2.17	1.60
Fe_2O_3	0.00	0.00	0.00	0.00	0.00	0.00	0.00	0.00	0.00	0.00	0.00
FeO	7.52	6.49	7.32	7.79	5.55	6.12	6.12	6.83	7.64	6.32	6.80
MnO	0.12	0.12	0.12	0.13	0.11	0.11	0.13	0.14	0.13	0.12	0.12
MgO	42.25	43.35	41.10	42.70	41.64	40.04	41.68	41.27	40.96	40.32	42.53
CaO	0.69	0.85	1.02	1.09	1.06	1.52	1.73	2.06	1.67	1.64	1.05
Na_2O	0.03	0.01	0.02	0.04	0.04	0.04	0.04	0.07	0.07	0.07	0.07
K_2O	0.00	0.00	0.00	0.00	0.06	0.07	0.06	0.02	0.03	0.02	0.02
P_2O_5	0.00	0.00	0.00	0.00	0.00	0.00	0.01	0.00	0.00	0.00	0.00
LOI	6.07	6.04	7.61	3.94	7.21	7.17	5.27	4.41	4.71	6.53	4.90
Total	99.84	99.95	99.92	99.87	99.92	99.93	99.99	99.99	99.97	100.06	99.95
Mg#	90.92	92.24	90.91	90.72	93.04	92.10	92.39	91.50	90.53	91.92	91.77
ppm											
Sc	4	3	4	6	3	4	4	5	7	5	4
Ga	1	0	0	0	0	1	0	1	2	1	1
Ni	2222	2153	2092	2223	1942	1863	1928	1897	2080	2035	2050
Co	112	112	106	111	109	104	110	114	108	108	111
Cr	2079	1572	1792	2410	1293	1590	1782	2117	2053	1626	1782
V	38	36	40	49	49	55	50	51	56	53	40
Ba	0	0	0	0	3	0	0	0	0	0	0
Pb	0	0	0	0	0	0	2	0	0	0	0
ICP-MS analysis (ppm)											
Y	0.559	0.699	0.701	0.891	0.969	1.210	1.702	1.900	2.123	2.079	
Zr	0.218	0.327	0.192	0.238	0.595	0.396	0.714	0.468	0.453	0.462	
Nb	0.257	0.266	0.209	0.329	0.525	2.218	0.802	0.320	0.179	0.235	
La	0.016	0.028	0.030	0.025	0.143	0.042	0.038	0.174	0.097	0.017	
Ce	0.027	0.040	0.030	0.031	0.269	0.077	0.095	0.273	0.196	0.045	
Pr	0.003	0.005	0.004	0.004	0.034	0.011	0.015	0.037	0.024	0.008	
Nd	0.012	0.019	0.016	0.013	0.133	0.047	0.081	0.162	0.113	0.056	
Sm	0.005	0.006	0.005	0.007	0.031	0.016	0.034	0.058	0.043	0.034	
Eu	0.002	0.003	0.002	0.003	0.007	0.006	0.016	0.023	0.025	0.020	
Gd	0.009	0.016	0.016	0.021	0.030	0.031	0.091	0.097	0.127	0.114	
Tb	0.002	0.004	0.004	0.006	0.007	0.010	0.023	0.026	0.029	0.029	
Dy	0.019	0.036	0.036	0.053	0.070	0.082	0.201	0.202	0.232	0.246	
Ho	0.006	0.011	0.012	0.016	0.019	0.030	0.048	0.050	0.056	0.059	
Er	0.024	0.047	0.047	0.064	0.074	0.109	0.159	0.165	0.195	0.193	
Tm	0.005	0.009	0.009	0.013	0.013	0.019	0.027	0.028	0.032	0.032	
Yb	0.046	0.071	0.071	0.097	0.112	0.142	0.195	0.190	0.221	0.228	
Lu	0.009	0.012	0.012	0.017	0.018	0.024	0.030	0.031	0.034	0.037	
Hf		0.007	0.005	0.005	0.016	0.056	0.027	0.021	0.027	0.023	
Ta	0.029	0.129	0.069	0.047	0.055	0.430	0.104	0.072	0.074	0.029	
Th		0.005	0.004	0.005	0.019	0.030	0.003	0.029	0.016		
U	0.008	0.003	0.001	0.002	0.033	0.007	0.016	0.020	0.019	0.004	

Hz: Harzburgite, Cpx-Hz: Clinopyroxene harzburgite, Lhrz: Lherzolite

in lherzolite. One of lherzolitic samples (sample 2-33) shows very high U/Th ratio (~ 20 × primitive mantle).

Concerning REEs, in harzburgite $(La/Sm)_N$ is from 2.03 to 3.62. $(Sm/Yb)_N$ and $(La/Yb)_N$ are in the ranges of 0.08 to 0.12 and 0.18 to 0.91, respectively. These normalized ratios imply that all harzburgitic samples show a decrease from HREE to MREE and enrichment of LREE compared to MREE making a concave upward REE patterns which is evident in Fig. 8. Also, in the case of lherzolite, $(La/Sm)_N$ ranges from 0.33 to 1.95. $(Sm/Yb)_N$ is from 0.13 to 0.34 and $(La/Yb)_N$ is in the range of 0.05 to 0.66. $(La/Sm)_N$ of lherzolitic samples exhibit that some samples (samples 4-10 and 6-38) show more prominent LREE enrichment and a steady decrease from MREE to LREE can be seen in the others (samples 2-20, 2-33 and 5-6). But the LREE contents of these samples (samples 2-20, 2-33 and 5-6) are higher than those of melting models i.e., these samples also show to some extent LREE

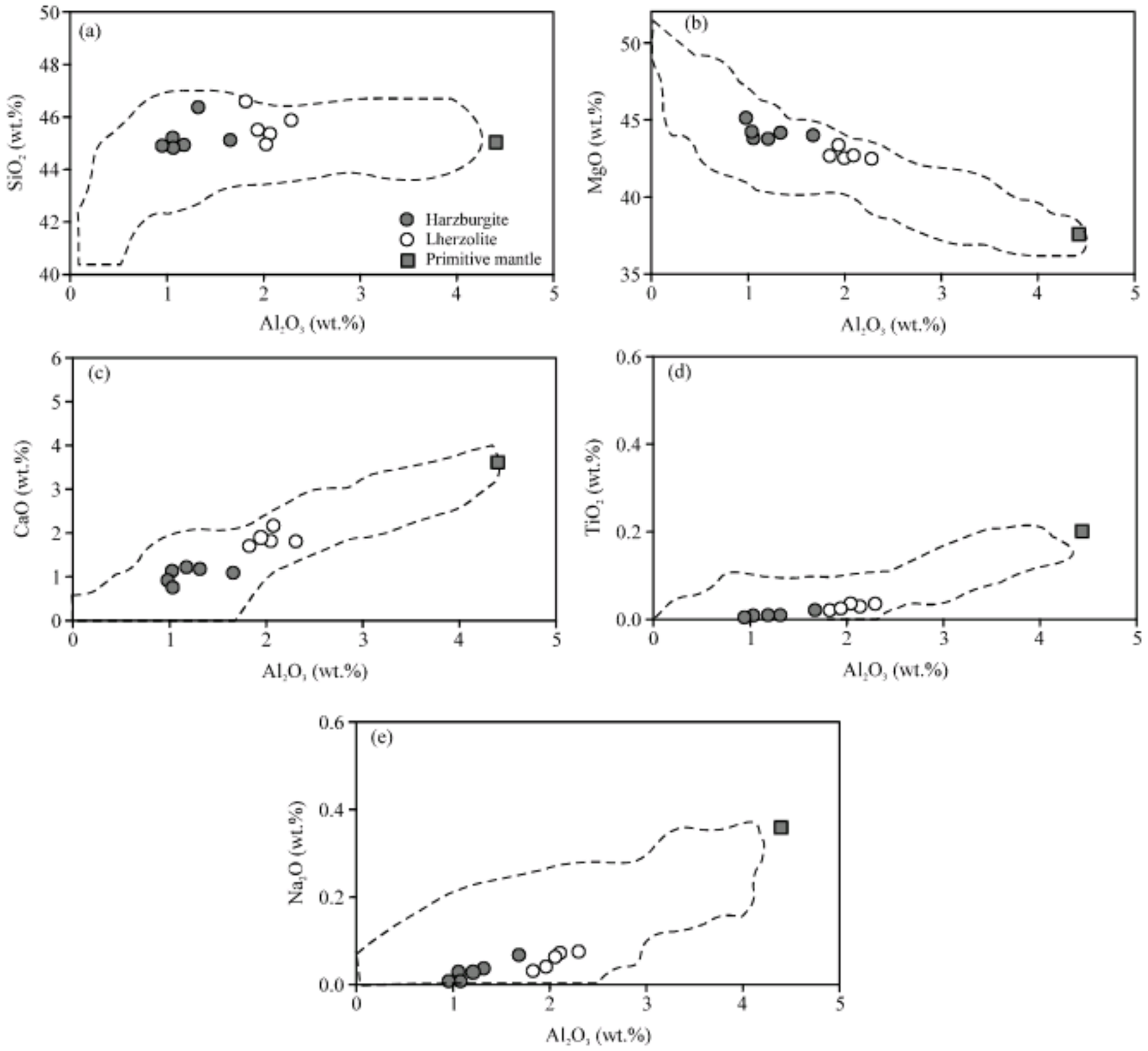

Fig. 6: (a-e) Major element oxides co-variation with Al_2O_3 in NOC mantle peridotites. The fields are variations of orogenic, abyssal and ophiolitic mantle peridotite (Bodinier and Godard, 2003). Primitive mantle composition from McDonough and Sun (1995)

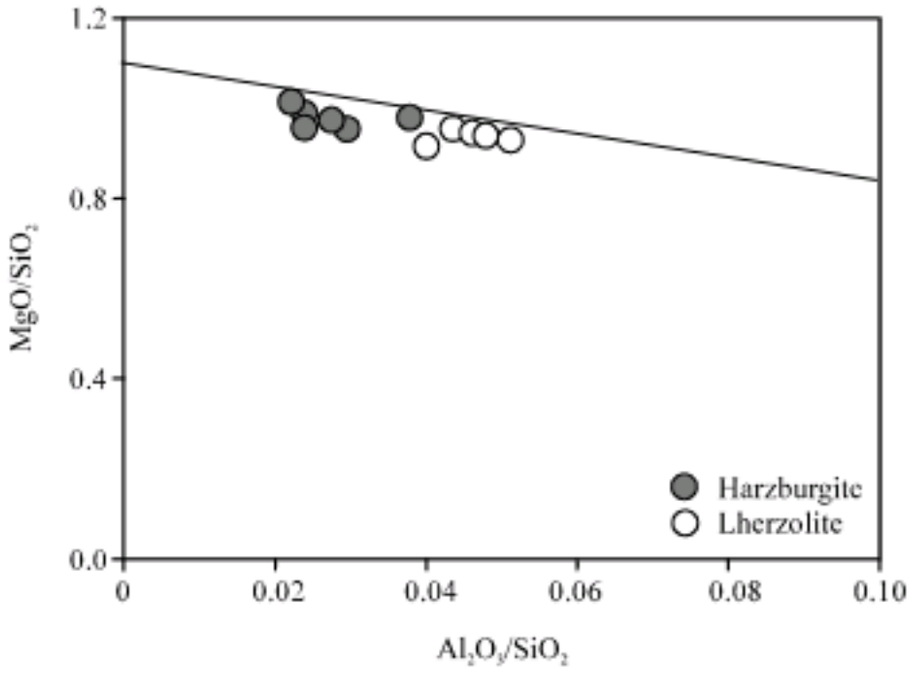

Fig. 7: MgO/SiO_2 vs. Al_2O_3/SiO_2 diagram. Terrestrial array from Jagoutz *et al.* (1979)

enrichment. Based on $(Sm/Yb)_N$ it is apparent that in harzburgite the slope of REE patterns from HREE to MREE show more steepness compared to lherzolite.

DISCUSSION

The enrichment of incompatible elements: Regarding Nb and Ta enrichments, this feature is seemingly a subject of deliberation. Among the four probable warehouse of incompatible trace elements in spinel peridotites i.e., major mineral phases (silicates and spinel), volatile-bearing accessory mineral phases, fluid-derived inclusions inside minerals and grain boundary components, Ti-rich oxides which appear as thin reaction layers coating the surfaces of spinel grains have been proposed as the main repository of Nb and Ta in spinel peridotites (Bedini and

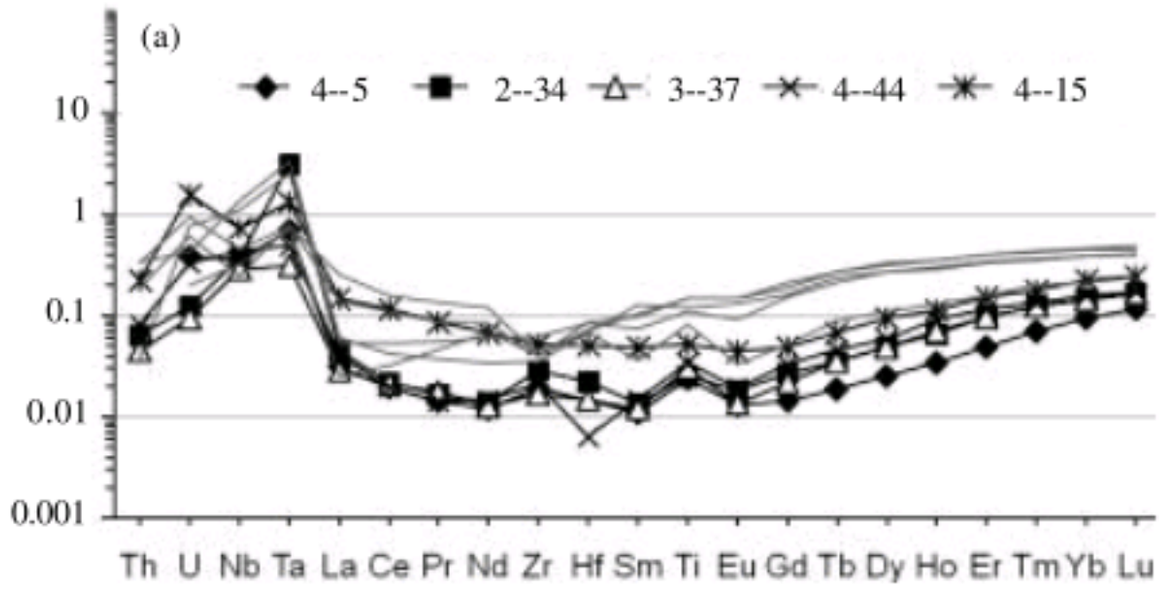

Fig. 8: PM-normalized REE and trace elements patterns for (a) harzburgite and (b) lherzolite. Normalizing values after Sun and McDonough (1989) Oman harzburgite from Godard *et al*. (2000)

Bodinier, 1999). In Fig. 8a and b, all the samples show more Ta enrichment relative to Nb which is evident from their Nb/Ta ratio. This can be due to higher incompatibility of Nb relative to Ta during melting which can favor lower Nb/Ta ratio in residual mantle peridotites. But as we noted before Nb and Ta are enriched in both harzburgite and lherzolite and Nb/Ta ratio in more depleted harzburgitic samples sometimes is higher respect to lherzolitic samples so the positive anomaly of these elements have been produced after melting process and governed by interaction of small fractions of Nb-Ta enriched melts having low Nb/Ta ratio. In Fig. 8b, the samples of Oman ophiolitic mantle harzburgite show the same HFSE enrichment, although the enrichment is less pronounced than that of NOC and low Nb/Ta is lacking. For it Godard *et al*. (2000) stated that enrichment of Th, Nb and Ta relative to LREE could hardly been explained by interaction with MORB melts but with tardily percolating small fractions of volatile rich fluids.

In addition to HFSE enrichment, NOC mantle peridotites display LREE enrichment. All the harzburgitic samples show a clear U-shaped REE profiles and in lherzolitic samples some samples show LREE enrichment over MREE (samples 4-10 and 6-38) but some of them (samples 2-20, 2-33 and 5-6) exhibit a continuous decrease of normalized REE abundances from MREE to LREE. In other words, lherzolitic samples show higher LREE dispersion (factor of 10 for La). U-shaped REE patterns in mantle peridotites are not uncommon and have been observed in orogenic (Bodinier *et al*., 1990), abyssal (Niu, 2004) and ophiolitic (Sharma and Wasserburg, 1996; Gruau *et al*., 1998) peridotites. In ophiolites, U-shaped REE patterns are almost restricted to highly refractory mantle peridotites (dunites and harzburgites) (Prinzhofer and Allègre, 1985; Sharma and Wasserburg, 1996). This feature can be shown by plotting LREE/MREE or LREE/HREE ratios versus HREE contents. Because LREE enrichment mostly appears in more depleted peridotites thereby ophiolitic mantle peridotites commonly exhibit negative correlation of LREE/MREE or LREE/HREE ratios versus HREE. In this regard, NOC samples appear to be somewhat identical to ophiolitic peridotites elsewhere because some of lherzolitic samples also represent LREE enrichment similar to harzburgitic ones. In Ce/Sm and Ce/Yb ratios vs. Yb abundances in NOC mantle peridotites (Fig. 9a, b), as a result of LREE enrichment in

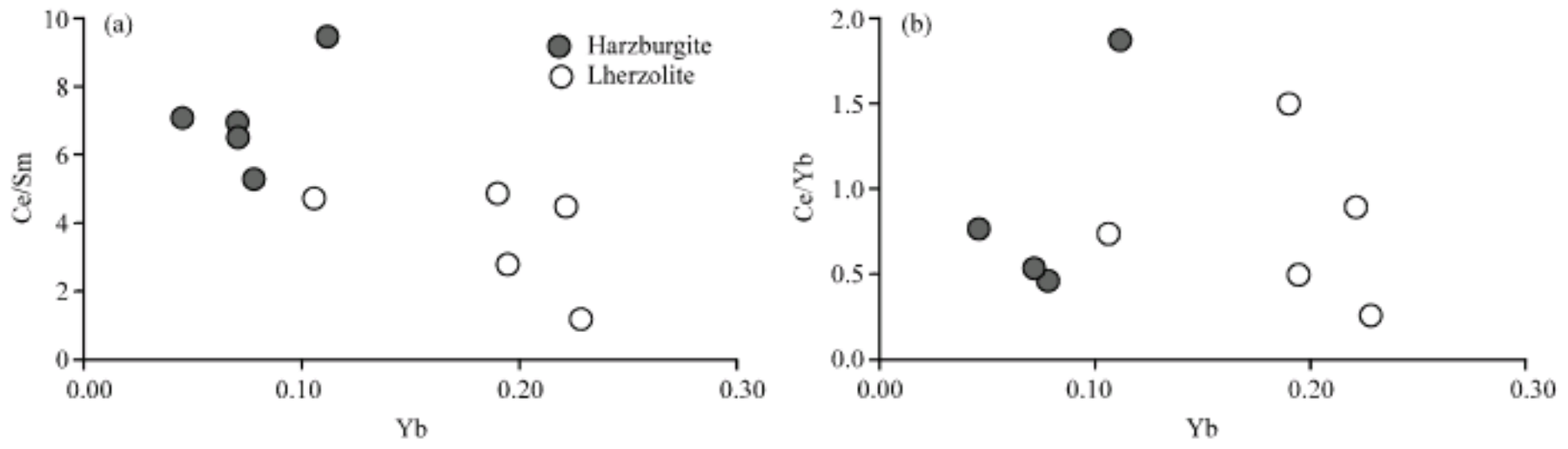

Fig. 9: (a) Ce/Sm and (b) Ce/Yb ratios vs. Yb

some of lherzolitic samples a clear negative correlation especially in the case of Ce/Yb versus Yb plot is lacking.

The origin of U-shaped REE patterns is a subject of contemplation. Many processes, for example, sequential disequilibrium melting model (Prinzhofer and Allègre, 1985), contamination by continental sources (Bodinier *et al*., 1990; Sharma and Wasserburg, 1996; Gruau *et al*., 1998), melt-rock interaction (Pearce *et al*., 2000; Niu, 2004), melt-rock interaction and hydrothermal processes (serpentinization) (Paulick *et al*., 2006) have been proposed for the origin of U-shaped REE patterns in mantle peridotites. Among these, sometimes one mechanism is more acceptable in a specific case but is hardly justifiable in other cases. For instance, LREE-enriched normalized REE patterns which is associated with low εNd(T) values and high $^{87}Sr/^{86}Sr(T)$ ratios can support contamination by continental sources (Sharma and Wasserburg, 1996; Gruau *et al*., 1998) but is not applicable to LREE-enriched patterns in refractory abyssal peridotites, or in altered abyssal peridotites, the role of alteration in LREE enrichment may be influential (Paulick *et al*., 2006) but have been rejected in orogenic peridotites (Frey *et al*., 1985). In NOC mantle peridotites, U-shaped REE patterns are not the result of serpentinization because there isn't any dependence between degree of LREE enrichment and that of serpentinization (LOI contents). Since both harzburgite and lherzolite of NOC display LREE enrichment so the relation between degree of depletion and LREE enrichment can be rejected. As high degree fractional melting will always yield normalized REE patterns with positive slopes therefore NOC mantle peridotites have been enriched after leaving melting region. Although, a batch melting process affecting already melt-depleted but metasomatically re-enriched peridotites would produce U-shaped REE patterns. Using the model of Sharma and Wasserburg (1996) (Fig. 10), the lherzolitic samples which display more LREE enrichment and all the harzburgitic samples plot on or close to the lines showing mantle

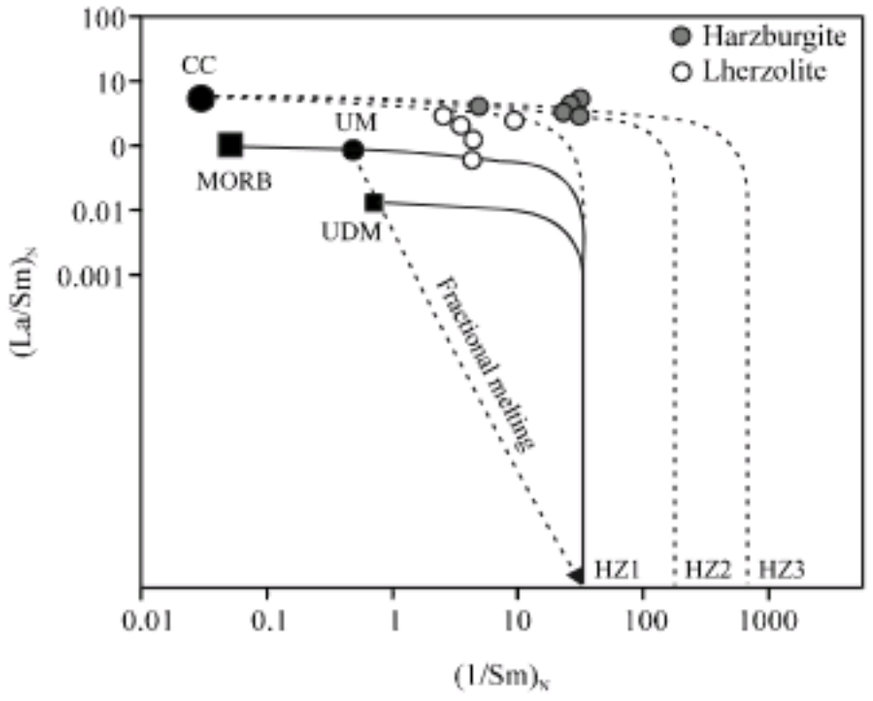

Fig. 10: Chondrite-normalized (Sun and McDonough, 1989) $(La/Sm)_N$ vs. $(1/Sm)_N$ diagram in mantle peridotites from NOC. The model showing contamination of residual harzburgites with MORB magmas or continental crust are from Sharma and Wasserburg (1996). MORB: Mid-ocean ridge basalts; UM: Upper mantle composition; CC: Continental crust composition: UDM: Ultra-depleted melt composition; HZ1, HZ2 and HZ3: Model harzburgite compositions. The UM-HZ1 dashed-line shows the covariation of $(La/Sm)_N$ and $(1/Sm)_N$ ratios due to equilibrium fractional melting in an upwelling upper mantle peridotite. The HZ1-CC, HZ2-CC and HZ3-CC dashed-curves represent contamination of three model harzburgites (HZ1, HZ2 and HZ3) with CC and the HZ1-UDM and HZ1-UM-MORB solid curves depict mixing of the HZ1 with UDM and MORB

contamination by continental crust components. Contamination by crustal sources could take place during mantle evolution in supra-subduction zone setting or after emplacement of the ophiolite complex onto the continent.

Some of lherzolitic samples which show lower LREE enrichment plot on the MORB-HZ1 or halfway between the CC-HZ and MORB-HZ1 curves. The MORB-HZ1 curve results from MORB-mantle interaction and this implicitly means that just lower LREE enrichment can be attained by melt-mantle interaction. Oppositely, Harte *et al.* (1993) proposed a percolative fractional crystallization mechanism by which highly LREE enrichment can be attained by melt-rock interaction. The exact nature of this percolating melt, however, is questioned; how can a LREE-depleted MORB make LREE enrichment in host peridotite? For this a LREE-enriched small melt fractions of evolved MORB has been proposed (Batanova *et al.*, 1998). Altogether, in terms of upper-mentioned model we can assume both of the processes; mantle-melt interaction for some slightly LREE-enriched samples and mantle-crustal source contamination for highly LREE-enriched samples. Another possible scenario is that the contamination by crustal source didn't take place uniformly throughout the mantle peridotites i.e., there is direct relationship between extent of LREE enrichment and the intensity of contamination by continental source. By this assumption the lherzolitic samples showing low LREE-enrichment have been less affected by circulating fluids. We must, however, acknowledge that better justification will be possible by further isotopic data.

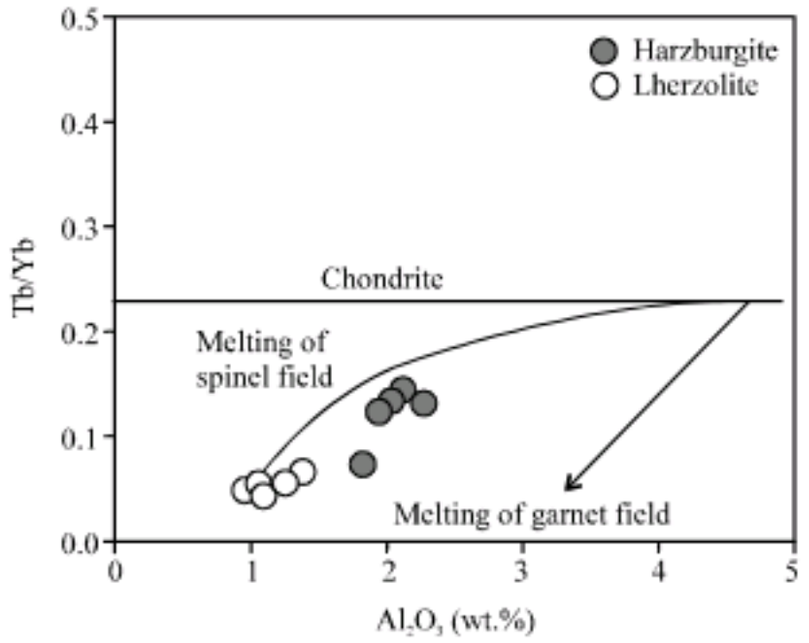

Fig. 11: Whole rock Tb/Yb vs. Al_2O_3 in mantle peridotites. The trends for melting in the spinel and garnet fields from Bodinier *et al.* (1988) and McDonough and Frey (1989)

Melting degrees: Here we can test the partial melting percents of NOC mantle peridotites. Petrographically, there is no metamorphic plagioclase in these mantle peridotites so their equilibration in spinel facies can be inferred which is also confirmed by the plot of whole rock data close to the spinel stability field melting trend in Fig. 11. Thus melting degrees could be estimated based on Cr# of spinel using the following equation:

$$F = 10 \times \ln (Cr\#) + 24 \text{ (Hellebrand } et\ al.\text{, 2001)}$$

In which F is melting degree (in percent) and Cr# is Cr/Cr+Al. Calculated melting degrees are 5 to 8% for lherzolite and 12.5 to 14.2% for harzburgite.

Chromite crystallization and the constraints on its geodynamic setting: The chromite deposits (chromitite) can be classified into two groups; stratiform and podiform chromitites. The podiform chromitites commonly appear as pod-shaped bodies near the crust–mantle boundary in the ophiolitic complexes (Lago *et al.*, 1982; Boudier and Nicholas, 1985).

The chromite is believed to be precipitated from the mantle-derived partial melts (Coleman, 1977). Magma composition from which chromite is crystallizing is one of the most important factors controlling the chemistry of chromite. In addition, the physical conditions such as pressure, temperature and fO_2 may have influence on the chemistry of the chromite (Irvine, 1965; Jaques and Green, 1980; Dick and Bullen, 1984; Roberts and Neary, 1993).

In NOC, based on chromite chemical composition, the nature of parental melt can be inferred using the contributory formulas of Maurel and Maurel (1982):

$$(Al_2O_3)^{2.42}_{melt}\ (wt.\%) = Al_2O_3{}_{spinel}\ (wt.\%) / 0.035$$

and

$$\text{Ln } (FeO/MgO)_{melt} = \ln (FeO/MgO)_{spinel} - 0.47 + 1.07 \times Y^{Al}_{spinel} - 0.64 \times Y^{Fe3+}_{spinel}$$

Where:

$Y^{Al}_{spinel} = Al/(Al + Cr + Fe^{3+})$

$Y^{Fe3+}_{spinel} = Fe^{3+}/(Fe^{3+} + Al + Cr)$

For NOC podiform chromitite the calculated Al_2O_3 content and FeO/MgO ratio of the melt in equilibrium with chromite is between 15-16 wt.% and 1.1 to 1.2, respectively.

Nearly high Al_2O_3 content and FeO/MgO ratio of the parental melt is in agreement with a MORB-type melt. This result is in accordance with the Fig. 12 in which NOC magmatic chromites due to their low Cr# plot within MORB field. Low Cr# (50 to 51) of magmatic chromites places them inside high-Al type of chromitites and in contrast with high-Cr chromites which crystallize from the melts with boninitic affinity, the high-Al ones originate from the tholeiitic melts (Zhou and Robinson, 1994).

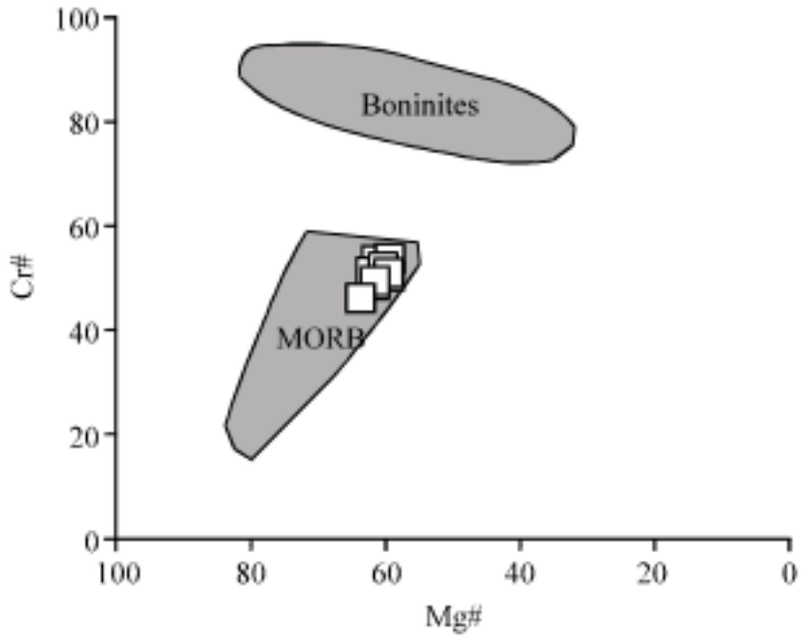

Fig. 12: Cr# vs. Mg# for chromites. Fields of MORB and boninite after Kepezhinskas *et al.* (1993)

The melt-rock or melt-melt interaction are the processes which have been invoked for the genesis of the podiform chromitites (Ballhaus, 1998; Proenza *et al*., 1999). The gradational changes from dunitic envelopes around podiform chromitites outward to harzburgite and lherzolite in the lithospheric mantle can be the result of melt-rock interaction (Kelemen *et al*., 1992). In the lithospheric mantle, Incongruent melting of orthopyroxene and dissolution of clinopyroxene via melt-rock interaction on the one side and the precipitation of olivine from the uprising melt because of the expanding of the liquidus volume of olivine with decreasing pressure on the other side (Kelemen *et al*., 1997) are the processes to form dunite around podiform chromitites. Melt-rock interaction can be enhanced where invading melt from deeper depth and the shallower host peridotite is out of equilibrium which can increase silica activity of interacting melt and modify melt chemistry toward boninitic affinity. Addition of a more primitive melt to upper-mentioned modified melt would cause crystallization of chromite via magma mixing (Irvine, 1965) or magma mingling (Ballhaus, 1998).

Notwithstanding the fact that melt-rock interaction could be facilitated in supra-subduction zone settings but geotectonic setting of podiform chromitites is still a matter of debate. In Oman ophiolite, based on negative Nb anomaly in analyzed mineral inclusions in chromites, Schiano *et al.* (1997) suggested a back-arc tectonic setting for its formation. Zhou *et al.* (1998) proposed an arc-related setting for high-Cr podiform chromitites and a nascent spreading center like back arc basin for high-Al ones. Contrastingly, Rollinson (2005) proposed a model in which both of low and high-Cr chromitites can form in the same tectonic setting so that the change in parental melt composition from tholeiitic to boninitic can be acquired by melt-rock interaction. The presence of hydrous mineral inclusions such as paragasite and phlogopite inside the chromites (Lorand and Ceuleneer, 1989) is another tool by which Matveev and Ballhaus (2002) stated that podiform chromites most plausibly form in a supra-subduction zone setting where high-fluid content of the melt can be expected to exsolve a separate water-rich fluid phase. It seems that chromitites can also be formed in mid-ocean ridge setting. Arai and Matsukage (1998) reported a chromitite micropod from Hess Deep (Oceanic Drilling Program (ODP) Leg 147). The same as ophiolitic podiform chromitites, the chromite grains from Hess Deep contain hydrous mineral inclusions. Although, chromites from the oceanic floor have low Cr# and high-Cr chromites (Cr#>0.7) is restricted to arc-related ophiolitic chromitites (Dick and Bullen, 1984; Arai and Matsukage, 1998).

Tectonic implications: NOC mantle comprises lowly depleted lherzolitic and moderate to highly depleted harzburgitic peridotites. Highly depleted nature of mantle peridotites can be assigned to supra-subduction zone setting in which fluid flux from subducting slab would facilitate re-melting of previously depleted mantle (Hirose and Kawamoto, 1995) or decompression melting beneath fast-spreading ridges inasmuch as higher spreading-rate of mid-ocean ridges induces higher melting degree in mantle (Niu and Hékinian, 1997). Given that the spinel chemistry is an expression of refractoriness degree of host peridotite, the composition of residual spinels in NOC harzburgite corresponds to abyssal peridotites or mildly refractory arc peridotites. Nevertheless, the Cr# of spinel in NOC harzburgite (31.6 to 37.5) is lower than that of many well-known supra-subduction zone ophiolites. For example in Oman ophiolite (Tamura and Arai, 2006), Cr# of spinel ranges from 62-76. On the other side, chemistry of chromite (magmatic spinel) is similar to high-Al type chromites rejecting its equilibration with boninitic parental melt. As noted before there are some gabbronoritic patches in NOC mantle peridotites recording crystallization sequence in which plagioclase has been preceded by ortho- and clinopyroxene. This type of crystallization sequence can be subjected to boninitic affinity of melt and is one of the common characteristics of mafic rocks with SSZ affinity (Pearce *et al.*, 1984; Hebert and Laurent, 1990). Making sense of these features will be possible by considering both MORB and SSZ tectonic settings.

CONCLUSION

NOC mantle tectonites include lherzolitic to harzburgitic peridotites which exhibit various and gradual refractoriness degree. Although, they are highly dismembered, higher re-equilibration temperature of

lherzolite compared to harzburgite denotes its deeper origin. Enrichment of HFSE in peridotite samples shows melt-mantle interaction and contamination with continental sources. Low to moderate melting degrees based on whole-rock and residual spinel chemistry and high-Al chemistry of magmatic spinel are dissimilar to the characteristics of typical arc-related peridotites. On the other hand, gabbronoritic intrusions cutting through mantle tectonites are signatures of SSZ setting.

ACKNOWLEDGMENTS

This article is the result of a Ph.D project (M. Delavari). Iranian ministry of Science, Research and Technology is acknowledged for financial support for a visinting scholar period in Ferrara, Italy. Special thanks to the staff and students from the Dipartimento di Scienze della Terra, Università di Ferrara, Italy. Mr. Ghasemi (one of the member of staff of Iranian ministry of Science, Research and Technology) is gratefully acknowledged for his useful administrative helps.

REFERENCES

Arai, S., 1994. Characterization of spinel peridotites by olivine-spinel compositional relationships: review and interpretation. Chem. Geol., 113: 191-204.

Arai, S. and K. Matsukage, 1998. Petrology of a chromitite micropod from Hess Deep, equatorial Pacific: A comparison between abyssal and alpine-type podiform chromitites. Lithos, 43: 1-14.

Arif, M. and M. Qasim Jan, 2006. Petrotectonic significance of the chemistry of chromite in the ultramafic-mafic complexes of Pakistan. J. Asian Earth Sci., 27: 628-646.

Ballhaus, C., 1998. Origin of podiform chromite deposits by magma mingling. Earth Planet. Sci. Lett., 156: 185-193.

Batanova, V.G., G. Suhr and A.V. Sobolev, 1998. Origin of geochemical heterogeneity in the mantle peridotites from the Bay of Islands Ophiolite (Newfoundland, Canada): Ion probe study of clinopyroxenes. Geochim. Cosmochim. Acta, 62: 853-866.

Bedini, R.M. and J.L. Bodinier, 1999. Distribution of incompatible trace elements between the constituents of spinel peridotite xenoliths: ICP–MS data from the East African Rift. Geochim. Cosmochim. Acta, 63: 3883-3900.

Bodinier, J.L., C. Dupuy and J. Dostal, 1988. Geochemistry and petrogenesis of Eastern Pyrenean peridotites. Geochim. Cosmochim. Acta, 52: 2893-2907.

Bodinier, J.L., G. Vasseur, J. Vernières, C. Dupuy and J. Fabriès, 1990. Mechanism of mantle metasomatism: Geochemical evidence from the Lherz orogenic peridotite. J. Petrol., 31: 597-628.

Bodinier, J.L. and M. Godard, 2003. Orogenic, Ophiolitic and Abyssal Peridotites. In: Treatise on Geochemistry, Carlson, R.W. (Ed.). Mantle and Core, Elsevier, ISBN: 0-08-043751-6.

Boudier, F. and A. Nicholas, 1985. Harzburgites and lherzolite subtypes in ophiolitic and oceanic environments. Earth Planet. Sci. Lett., 76: 84-92.

Brey, G.P. and T.P. Köhler, 1990. Geothermobarometry in four-phase lherzolite II. New thermobarometers and practical assessment of existing thermobarometers. J. Petrol., 31: 1353-1378.

Büchl, A., G. Brügmann and V.G. Batanova, 2004. Formation of podiform chromitite deposits: Implications from PGE abundances and Os isotopic compositions of chromites from the Troodos complex, Cyprus. Chem. Geol., 208: 217-232.

Coleman, R.G., 1977. Ophiolites: Ancient Oceanic Lithosphere? Springer, New York.

Dick, H.J.B. and T. Bullen, 1984. Chromian spinel as a petrogenetic indicator in abyssal and alpine-type peridotites and spatially associated lavas. Contrib. Mineral. Petrol., 86: 54-76.

Frey, F.A., C.J. Suen and H.W. Stockman, 1985. The Ronda high temperature peridotite: Geochemistry and petrogenesis. Geochim. Cosmochim. Acta, 49: 2469-2491.

Godard, M., D. Jousselin and J.L. Bodinier, 2000. Relationships between geochemistry and structure beneath a palaeo-spreading centre: A study of the mantle section in the Oman ophiolite. Earth Planet. Sci. Lett., 180: 133-148.

Gruau, G., J. Bernard-Griffiths and C. Lécuyer, 1998. The origin of U-shaped rare earth patterns in ophiolite peridotites: Assessing the role of secondary alteration and melt/rock reaction. Geochim. Cosmochim. Acta, 62: 3545-3560.

Harte, B., R.H. Hunter and P.D. Kinny, 1993. Melt geometry, movement and crystallization, in relation to mantle dykes, veins and metasomatism. Phil. Trans. R. Soc. London, 342: 1-21.

Hebert, R. and R. Laurent, 1990. Mineral chemistry of the plutonic section of the Troodos Ophiolite: New constraints for genesis of arc-related ophiolites, in Ophiolites Oceanic Crustal Analogues. Proceedings of the Symposium Troodos 1987, 1990, Geol. Survey Dep., Nicosia, Cyprus, pp: 149-163.

Hellebrand, E., J.E. Snow, H.J.B. Dick and A.W. Hofmann, 2001. Coupled major and trace elements as indicators of the extent of melting in mid-ocean-ridge peridotites. Nature, 410: 677-681.

Hirose, K. and T. Kawamoto, 1995. Hydrous partial melting of lherzolite at 1 GPa: The effect of H_2O on the genesis of basaltic magmas. Earth Planet. Sci. Lett., 133: 463-473.

Irvine, T.N., 1965. Chromium spinels as a petrogenetic indicator. I, Theory. Can. J. Earth Sci., 2: 648-672.

Ishii, T., P.T. Robinson, H. Maekawa and R. Fiske, 1992. Petrological studies of peridotites from diapiric serpentinite seamounts in the Izu-Ogasawara-Mariana forearc, LEG125. Proceedings of the Ocean Drilling Program, 1992, Scientific Results, pp: 445-485.

Jagoutz, E., H. Palme, H. Baddenhausen, K. Blum, M. Cendales, G. Dreibus, B. Spettel, V. Lorentz and H. Wänke, 1979. The abundance of major, minor and trace elements in the Earth's mantle as derived from primitive ultramafic nodules. Proceedings of the 10th Lunar and Planetary Science Conference, 1979, Houston, Tex., New York, pp: 2031-2050.

Jaques, A.L. and D.H. Green, 1980. Anhydrous melting of peridotite at 0-15 kbar and the genesis of tholeiitic basalts. Contrib. Mineral. Petrol., 73: 287-310.

Johnson, K.T.M., H.J.B. Dick and N. Shimizu, 1990. Melting in the oceanic upper mantle: An ion microprobe study of diopsides in abyssal peridotites. J. Geophys. Res., 95: 2661-2678.

Kamenetsky, V.S., A.J. Crawford and S. Meffre, 2001. Factors controlling chemistry of magmatic spinel: An empirical study of associated olivine, Cr-spinel and melt inclusions from primitive rocks. J. Petrol., 4: 655-671.

Karipi, S., B. Tsikouras, K. Hatzipanagiotou and T.A. Grammatikopoulos, 2007. Petrogenetic significance of spinel-group minerals from the ultramafic rocks of the Iti and Kallidromon ophiolites (Central Greece). Lithos, 99: 136-149.

Kelemen, P.B., H.J.B. Dick and J.E. Quick, 1992. Formation of harzburgite by ervasive melt/rock reaction in the upper mantle. Nature, 358: 635-641.

Kelemen, P., G. Hirth, N. Shimizu, M. Spiegelman and H.J.B. Dick, 1997. A review of melt migration processes in the adiabatically upwelling mantle beneath oceanic spreading ridges. Phil. Trans. R. Soc. London A, 355: 283-318.

Kepezhinskas, P.K., R.N. Taylor and H. Tanaka, 1993. Geochemistry of plutonic spinels from the north Kamchatka arc: Comparisons with spinels from other tectonic settings. Mineral. Mag., 57: 575-589.

Lachance, G.R. and R.J. Trail, 1966. Practical solution to the matrix problem in X-ray analysis. Can. Spectrosc., 11: 43-48.

Lago, B.L., M. Rabinowicz and A. Nicholas, 1982. Podiform chromite ore bodies. A genetic model. J. Petrol., 23: 103-125.

Lorand, J.P. and G. Ceuleneer, 1989. Silicate and base metal sulfide inclusions in chromites from the Maqsad area (Oman ophiolite, Gulf of Oman): A model for entrapment. Lithos, 22: 173-190.

Matveev, S. and C. Ballhaus, 2002. Role of water in the origin of podiform chromitite deposits. Earth Planet. Sci. Lett., 203: 235-243.

Maurel, C. and P. Maurel, 1982. Etude expérimentale de la distribution de I'aluminum entre bain silicaté basique et spinelle chromifère. Implications pétrogénétiques: Teneur en chrome des spinelles. Bull. Min., 105: 197-202.

McDonough, W.F. and F.A. Frey, 1989. Rare Earth Elements in Upper Mantle Rocks. In: Geochemistry and Mineralogy of Rare Earth Elements, Lipin, B.R. and G.A. McKay (Eds.). Mineral. Soc. Am., Reviews in Mineralogy, Washington, DC., pp: 99-145.

McDonough, W.F. and S.S. Sun, 1995. The composition of the Earth. Chem. Geol., 120: 223-253.

Morimoto, N., 1989. Nomenclature of pyroxenes. Can. Mineralogist, 27: 143-156.

Niu, Y. and R. Hékinian, 1997. Spreading-rate dependence of the extent of mantle melting beneath ocean ridges. Nature, 385: 326-329.

Niu, Y., 2004. Bulk-rock major and trace element compositions of abyssal peridotites: Implications for mantle melting, melt extraction and post-melting processes beneath mid-ocean ridges. J. Petrol., 45: 2423-2458.

Pagé, P., J.H. Bédard, J.M. Schroetter and A. Tremblay, 2007. Mantle petrology and mineralogy of the thetford mines ophiolite complex. Lithos, 100: 255-292.

Parkinson, I.J. and J.A. Pearce, 1998. Peridotites from the Izu-Bonin-Mariana forearc (ODP Leg 125): Evidence for mantle melting and melt-mantle interaction in a supra-subduction zone setting. J. Petrol., 39: 1577-1618.

Paulick, H., W. Bach, M. Godard, J.C.M. De Hoog, G. Suhr and J. Harvey, 2006. Geochemistry of abyssal peridotites (Mid-Atlantic Ridge, 15°20'N, ODP Leg 209): Implications for fluid/rock interaction in slow spreading environments. Chem. Geol., 234: 179-210.

Pearce, J.A., S.J. Lippard and S. Roberts, 1984. Characteristics and tectonic significance of supra-subduction zone ophiolites. Geol. Soc. London Special Publ., 16: 77-94.

Pearce, J.A., P.F. Barker, S.J. Edwards, I.J. Parkinson and P.T. Leat, 2000. Geochemistry and tectonic significance of peridotites from the South Sandwich arc-basin system, South Atlantic. Contrib. Mineral. Petrol., 139: 36-53.

Prinzhofer, A. and C.J. Allègre, 1985. Residual peridotites and the mechanisms of partial melting. Earth Planet. Sci. Lett., 74: 251-265.

Proenza, J., F. Gervilla, J.C. Melgarejo and J.L. Bodinier, 1999. Al-and Cr-rich chromitites from the Mayari-Baracoa ophiolitic belt (Eastern Cuba): Consequence of interaction between volatile-rich melts and peridotites in suprasubduction mantle. Econ. Geol., 94: 547-566.

Roberts, S. and C.R. Neary, 1993. Petrogenesis of ophiolitic chromitite. Geol. Soc. London Special Publ., 76: 257-272.

Rollinson, H., 2005. Chromite in the mantle section of the Oman ophiolite: A new genetic model. Island Arc., 14: 542-550.

Schiano, P., R. Clocchiatti, J.P. Lorand, D. Massare, E. Deloule and M. Chaussidon, 1997. Primitive basaltic melts included in podiform chromites from the Oman Ophiolite. Earth Planet. Sci. Lett., 146: 489-497.

Sharma, M. and G.J. Wasserburg, 1996. The neodymium isotopic compositions and rare earth patterns in highly depleted ultramafic rocks. Geochim. Cosmochim. Acta, 60: 4537-4550.

Sun, S.S. and W.F. McDonough, 1989. Chemical and isotopic systematics of ocean basalts: implications formantle composition and processes. Geol. Soc. London Special Publ., 42: 313-346.

Takazawa, E., T. Okayasu and K. Satoh, 2003. Geochemistry and origin of the basal lherzolites from the northern Oman ophiolite (northern Fizh block). Geochem. Geophys. Geosyst., 4: 8605-8605.

Tamura, A. and S. Arai, 2006. Harzburgite-dunite-orthopyroxenite suite as a record of supra-subduction zone setting for the Oman ophiolite mantle. Lithos, 90: 43-56.

Tirrul, R., I.R. Bell, R.J. Griffis and V.E. Camp, 1983. The Sistan suture zone of Eastern Iran, Geol. Soc. Am. Bull., 94: 134-156.

Tirrul, R., J.W. Johns, N.O. Willoughby, V.E. Camp, R.J. Griffis, I.R. Bell and H.M. Meixner, 1989. Geological map of Nehbandan. Geological Survey of Iran.

Wells, P.R.A., 1977. Pyroxene thermometry in simple and complex systems. Contrib. Mineral Petrol., 62: 129-139.

Witt-Eickschen, G.E. and H.A. Seck, 1991. Solubility of Ca and Al on Orthopyroxene from Spinel Peridotite: An improved version of an empirical geothermometer. Contrib. Mineral. Petrol., 106: 431-439.

Zhou, M.F. and P.T. Robinson, 1994. High-chromium and high-aluminum podiform chromitites, western China: Relationship to partial melting and melt/rock interaction in the upper mantle. Int. Geol. Rev., 36: 678-686.

Zhou, M.F., P.T. Robinson, J. Malpas and Z. Li, 1996. Podiform chromitites in the luobusa ophiolite (SouthernTibet): Implications for melt-rock interaction and chromite segregation in the upper mantle. J. Petrol., 37: 3-21.

Zhou, M.F., M. Sun, R.R. Keays and R.W. Kerrich, 1998. Controls of platinum-group elemental distributions of podiform chromitites: A case study of high-Cr and high-Al chromitites from Chinese orogenic belts. Geochim. Cosmochim. Acta, 62: 677-688.